LITERATURE CITED

1. L. P. Orlov and V. E. Fertman, Magnetic-Fluid Seals for Rotating Shafts (Preprint of the A. V. Lykov Institute of Heat and Mass Transfer of the Academy of Sciences of the Belorussian SSR, No. 8) [in Russian], ITMO AN BSSR, Minsk (1979).
2. L. P. Orlov, A. K. Sinitsyn, and V. E. Fertman, Inzh.-Fiz. Zh., 42, No. 1, 58-65 (1982).
3. A. N. Veslovich, S. A. Demchuk, V. I. Kordonskii, and V. E. Fertman, in: Abstr. All-Union Symp. Hydrodynamics and Heat Physics of Magnetic Fluids [in Russian], Salaspils (1980), pp. 97-104.
4. R. E. Rosensweig, R. Kaiser, and G. Miskolszy, J. Colloid Interface Sci., 29, No. 4, 580-585 (1969).
5. V. A. Chernobai, Problems of the Mechanics of Magnetic Fluids [in Russian], Minsk (1981), pp. 110-116.
6. G. É. Kronkalns, M. M. Maiorov, and V. E. Fertman, Magn. Gidrodin., No. 2, 38-42 (1984).
7. A. A. Samarskii, Theory of Difference Schemes [in Russian], Moscow (1983).
8. B. M. Berkovskii, A. N. Vislovich, and B. É. Kashevskii, The Magnetic Fluid as a continuum with Internal Degrees of Freedom (Preprint of the A. V. Lykov Institute of Heat and Mass Transfer of the Academy of Sciences of the Belorussian SSR, No. 4) [in Russian], ITMO AN BSSR, Minsk (1980).
9. V. A. Novikov, A. K. Sinitsyn, and V. E. Fertman, in: Proc. Third All-Union School-Sem. Magnetic Fluids (Ples, 1983) [in Russian], Moscow (1983), pp. 186-187.
10. V. A. Novikov, A. K. Sinitsyn, and V. E. Fertman, in: Abstr. Eleventh Riga Conf. Magnetohydrodynamics [in Russian], Vol. 3, Salaspils (1984), pp. 119-122.
11. V. A. Chernobai, "Thermal and hydrodynamic processes in high-speed magnetic-fluid seals: structural design," Author's Abstract of Candidate's Dissertation, Engineering Sciences, Moscow (1984).
12. L.-H. Lee, Probl. Treniya, 100, No. 2, 132-142 (1978).

HYDRAULIC DRAG IN TURBULENT COOLANT FLOW IN A POROUS CABLE

V. A. Babenko

UDC 532.517.4+536.48

The hydrodynamics and heat transfer in the cooling of an electrical cable by radical coolant filtration are studied.

The constructional scheme of the cable is shown in Fig. 1. There are two coolant channels, of circular and annular cross section. Attachments that completely or partially cover the channel force the coolant to filter in the radial direction through the permeable structure formed by the current-carrying strands, the porous insulation, and the supporting base.

The model of a porous body with equivalent permeability, heat conduction, and heat liberation is used for mathematical modeling of the hydrodynamic and thermal processes in the permeable structure. The current-conducting part is cooled on account of heat transfer at the surfaces and intrapore heat transfer.

The hydrodynamics in the heat exchanger is modeled using channel-averaged equations of mass and momentum balance.

The momentum-balance equation is written for the tube

$$\frac{d}{dx^*}\left(\beta_{\text{т}}\bar{\rho}^*_{\text{т}}\bar{u}^{*2}_{\text{т}}S^*_{\text{т}} + P^*_{\text{т}}S^*_{\text{т}}\right) = -\tau^{a^*}2\pi a^* \tag{1}$$

and for the annular channel

$$\frac{d}{dx^*}\left(\beta_{\text{с}}\bar{\rho}^*_{\text{с}}\bar{u}^{*2}_{\text{с}}S^*_{\text{с}} + P^*_{\text{с}}S^*_{\text{с}}\right) = -\tau^{b^*}2\pi b^* - \tau^{c^*}2\pi c^*. \tag{2}$$

A. V. Lykov Institute of Heat and Mass Transfer, Academy of Sciences of the Belorussian SSR, Minsk. Translated from Inzhenerno-Fizicheskii Zhurnal, Vol. 51, No. 3, pp. 375-383, September, 1986. Original article submitted May 5, 1985.

 0022-0841/86/5103-1016$12.50

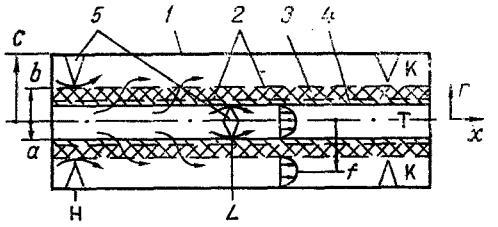

Fig. 1. Porous cable: 1) sheath; 2) current conductors; 3) porous electrical insulation; 4) supporting base; 5) blocking attachments.

The rate of transfer through the porous cylindrical wall is determined according to Darcy's law

$$a^*\rho^{a^*}v^{a^*} = b^*\rho^{b^*}v^{b^*} = \frac{K^*}{\nu^* \ln b/a}\,(P_T^* - P_C^*). \tag{3}$$

The mass-balance equations in the channels take the form

$$\frac{d}{dx^*}\,(\bar{\rho}_T^*\,\bar{u}_T^* S_T^*) = -\rho^{a^*}v^{a^*}2\pi a^*, \tag{4}$$

$$\frac{d}{dx^*}\,(\bar{\rho}_C^*\,\bar{u}_C^* S_C^*) = \rho^{b^*}v^{b^*}2\pi b^*. \tag{5}$$

Next, Eqs. (1)-(5) are brought to dimensionless form, referring the linear dimensions to the length scale $L^* = ((S_T^* = S_C^*)/2\pi)^{1/2}$, the channel cross section to the total cross section $S_\Sigma^* = S_T^* + S_C^*$, the density to ρ_0^*, the velocity to $u_0^* = G^*/S_\Sigma^*\rho_0^*$, and the tangential stress and pressure to $\rho_0^* u_0^{*2}$. Let $\omega_i = \rho_i u_i S_i, i=T,C$ denote the proportion of the mass flow rate and $j = \rho^a v^a a$ the dimensionless transverse mass flow rate.

The pressure is now eliminated from Eqs. (1)-(5). Differentiating Eq. (3) with respect to x^*, assuming constant properties, and neglecting the derivatives of the momentum-flow coefficients, an equation for j is obtained

$$\frac{1}{KN}\,\frac{dj}{dx} = 2\left(\frac{\beta_T \bar{u}_T}{S_T} + \frac{\beta_C \bar{u}_C}{S_C}\right) j - \frac{a u_\tau^{a^2}}{S_T} + \frac{b u_\tau^{b^2}}{S_C} + \frac{c u_\tau^{c^2}}{S_C}. \tag{6}$$

To calculate the coefficients characteristing the flow structure, the presence of local self-similarity of the flow in regions adjacent to the walls a, b, c is assumed, in the form $u^+ = f(y^+, v_w^+)$ in hydrodynamic similarity variables.

The dynamic shear velocities $u_\tau{}^a$ and $u_\tau{}^b$ are determined from the integral mass-balance equations in the channels

$$\omega_T = \int_0^{a^+} u^+ r^+ dr^+/(u_\tau^a N^2), \tag{7}$$

$$\omega_C = \omega_b + \omega_c = \int_{b^+}^{f^+} u^+ r^+ dr^+/(u_\tau^b N^2) + \int_{f^+}^{c_+} u^+ r^+ dr^+/(u_\tau^c N^2). \tag{8}$$

The relation for $u_\tau{}^c$ is obtained from the momentum-balance equation in the region c ($f \leqslant r \leqslant c$):

$$\int_f^c 2u\,\frac{\partial}{\partial x}\,(ur)\,dr - u_f \int_f^c \frac{\partial}{\partial x}\,(ur)\,dr = -\frac{dP_C}{dx}\,S_c - c u_\tau^{c^2}. \tag{9}$$

The left-hand side of Eq. (9) is expressed in terms of the hydrodynamic similarity variables and transformed by integration by parts

$$\int_f^c 2u\,\frac{\partial}{\partial x}\,(ur)\,dr - u_f \int_f^c \frac{\partial}{\partial x}\,(ur)\,dr = \tag{10}$$

$$= \frac{1}{N^2}\left[\int_0^{c^+-f^+} 2u^+ \frac{\partial}{\partial x}(u^+(c^+-y^+))\,dy^+ - u_{c_f}^+ \int_0^{c^+-f^+} \frac{\partial}{\partial x}(u^+(c^+-y^+))\,dy^+\right] =$$

$$= \frac{du_\tau^c}{dx}\frac{1}{u_\tau^c N^2}\left[\int_0^{c^+-f^+} 2u^+ \frac{\partial}{\partial y^+}(u^+(c^+-y^+))\,y^+dy^+ -\right.$$

$$\left. - u_{c_f}^+ \int_0^{c^+-f^+} \frac{\partial}{\partial y^+}(u^+(c^+-y^+))\,y^+dy^+ + 2c^+ \int_0^{c^+-f^+} u^{+2}\,dy^+ - c^+u_{c_f}^+ \int_0^{c^+-f^+} u^+dy^+\right] = \frac{du_\tau^c}{dx}\frac{I_{1_c}}{u_\tau^c}.$$

Here

$$I_{1_c} = \frac{1}{N^2}\left[c^+ \int_0^{c^+-f^+} u^{+2}\,dy^+ - u_{c_f}^+ \int_0^{c^+-f^+} u^+y^+dy^+\right].$$

Eliminating the pressure gradient from Eqs. (2) and (9), a differential equation for $u_\tau{}^c$ is obtained

$$\frac{du_\tau^c}{dx} = (2\beta_c\bar{u}_c S_c j + bu_\tau^{b^2}S_c - cu_\tau^{c^2}S_b)\,u_\tau^c I_{1_c}^{-1} S_c^{-1}. \tag{11}$$

The position of the maximum-velocity radius r = f in the annular channel is determined from the junction of the velocity profiles from walls b and c at this point

$$u_{b_f}^+ u_\tau^b = u_{c_f}^+ u_\tau^c. \tag{12}$$

The momentum-balance equation in the tube is transformed using the mass-conservation equation in Eq. (4)

$$\frac{dP_T}{dx} = 2\beta_T \frac{\omega_T}{S_T^2} j - \frac{au_\tau^{a^2}}{S_T}. \tag{13}$$

Equations (13) and (3) serve for the calculation of the pressure field in the heat exchanger. The general calculation scheme involves solving a system of ordinary differential equations – Eqs. (4), (6), (10), and (13) – and algebraic equations – Eqs. (7), (8), and (12). The integrals in Eqs. (7), (8), and (10) may be calculated according to an analytical formula from the specific form of the self-similar velocity profile in the wall region (wall law).

The following wall law is specified

$$u^+ = \begin{cases} \dfrac{\exp(v_w^+ y^+) - 1}{v_w^+} & \text{when } y^+ < y_{1a}^+, \\ z + \dfrac{v_w^+}{4} z^2 & \text{when } y^+ > y_{1a}^+, \end{cases} \tag{14}$$

where $y_{1a}{}^+$ is the thickness of the dynamic sublayer; $\chi = 0.4$ is the Karman constant; $z = 1/\chi \ln y^+ + B^+$. The constant B^+ depends on the injection–suction rate and is 5.5 when $v_w{}^+ = 0$. The expressions used to calculate $y_{1a}{}^+(v_w{}^+)$ and $B^+(v_w{}^+)$ are [1]

$$\frac{y_{1a}^+}{v_w^+}\left[\exp(v_w^+ y_{1a}^+) - 1\right] = (11{,}635)^2, \tag{15}$$

$$B^+ = \frac{2}{v_w^+}\left(\exp\left(\frac{v_w^+ y_{1a}^+}{2}\right) - 1\right) - \frac{1}{\chi}\ln y_{1a}^+. \tag{16}$$

Equation (15), which is transcendental with respect to $y_{1a}{}^+$, serves as the hypothesis for determined determining $y_{1a}{}^+$, while Eq. (16) for B^+ is written on the basis of continuous splicing of the velocity profiles in the laminar sublayer and the turbulent layer when $y^+ = y_{1a}{}^+$.

Substituting the wall law in Eq. (14) into Eqs. (7), (8), and (12) in each of the regions of integration a, b, and c gives Eq. (7), which is transcendental with respect to $u_\tau{}^a$, and the system of Eqs. (8) and (12), which are transcendental with respect to $u_\tau{}^b$ and f. The algorithm for their solution is now described.

Approximations for $u_\tau{}^a$, $u_\tau{}^b$, and f are specified on the basis of the previous history of the flow. Equation (15) for $y^+{}_{i1a,i=a,b}$ is solved iteratively by the Newton's method; this requires two or three iterations. Calculating the integrals in Eqs. (7) and (8) according to the velocity profile in Eq. (14), the expression obtained for $\omega_{i,i=a,b,c}$ is

$$\omega = u_\tau^2 [J_3(y_{1a}, r_w, R_w) - J_3(0, r_w, R_w)] + u_\tau [J_1(y_E, z_E^p, r_w) - J_1(y_{1a}, z_{1a}^{1a}, r_w)] + [J_2(y_E, z_E^p, r_w, R_w) - J_2(y_{1a}, z_{1a}^p, r_w, R_w)], \quad (17)$$

where $r_w = (a, b, c)_{a,b,c}$; $R_w = (-R, R, 0)_{a,b,c}$;

$$J_1(y, z, r_w) = \left[y(r_w \mp y/2) z - \frac{y}{\chi} (r_w \mp y/4) \right];$$

$$J_2(y, z, r_w, R_w) = \frac{R_w}{4Nr_w} \left[y(r_w \mp y/2) z^2 - \frac{y}{\chi} (r_w \mp y/4) 2z + \frac{y}{\chi^2} (r_w \mp y/8) 2 \right];$$

$$J_3(y, r_w, R_w) = N \left[\frac{-yr_w(r_w \mp y/2)}{R_w} + \frac{r_w^2}{R_w^2} \exp\left(\frac{R_w y}{r_w}\right) \left(r_w \mp y + \frac{r_w}{R_w}\right) \right],$$

and the superscript p denotes the value from the preceding iteration.

The dynamic shear velocities $u_\tau{}^a$, $u_\tau{}^b$ are found from Eq. (17), which is quadratic in $u_\tau{}^i$, i = a, b; iteration is necessary here (usually no more than three or four iterations), since u_τ appears in the coodinate z. The quadratic Eq. (17) has one positive root. The other root is negative and of no significance here. In region c, knowing $u_\tau{}^c$, the dependent variable of Eq. (11), Eq. (17) permits the determination of ω_c and $\omega_b = \omega_C - \omega_c$.

The position of the velocity maximum in the annular channel r = f separating the channel from zones b and c is determined iteratively from Eq. (12) by Newton's method at fixed $u_\tau{}^b$.

After obtaining the new values $u_\tau{}^a$, $u_\tau{}^b$, f, the whole cycle of calculations, consisting in the successive determination of $y^+{}_{i1a,i=a,b,c}$, $u_\tau{}^a$, $u_\tau{}^b$, ω_c, ω_b, and f is repeated so as to monitor the accuracy. Despite the presence of several iterative procedures, this algorithm is more convenient for calculations and more reliable than the use of standard numerical procedures for solving systems of algebraic transcendental equations. The calculations are made according to explicit formulas.

It is simple to obtain explicit formulas also for calculating the momentum-flux coefficients β_T and β_C; however, in the given case it is simpler to perform numerical integration after determining all the characteristics of the velocity profile.

The integrals appearing in I_{1c} need only be calculated in region c, for which $v_w{}^+ = 0$, while the first line in Eq. (14) is replaced by $u^+ = y^+$ and the second by $u^+ = z$. Integration gives

$$I_{1c} = c^2 u_\tau^{c^2} \left[\frac{(c-f)}{c} \left(\frac{2}{\chi^2} - \frac{2}{\chi} z_E + z_E^2 \right) - \frac{y^+_{c_{1a}}}{c^+} \left(\frac{2}{\chi^2} - \frac{2}{\chi} y^+_{c_{1a}} + y^{+^2}_{c_{1a}} \right) - \right.$$
$$- \frac{z_E}{2} \left(\left(\frac{c-f}{c} \right)^2 \left(-\frac{1}{2\chi} + z_E \right) - \left(\frac{y^+_{c_{1a}}}{c^+} \right)^2 \left(-\frac{1}{2\chi} + y^+_{c_{1a}} \right) \right) + \quad (18)$$
$$\left. + (c^+ - z_E) \left(\frac{y^+_{c_{1a}}}{c^+} \right)^2 \frac{y^+_{c_{1a}}}{3} \right].$$

The theoretical model is tested by comparison with well-known data from flow in a tube and an annular gap in conditions where leakage through the wall does, and does not, occur. The theoretical dependences $C_{FT} = f(Re_T)$ and $C_{FC} = f(Re_C)$ coincide within limits of 2% with the well-known Filonenko–Blasius dependence [2] for a tube and with the analogous dependence for an annular channel [3]. The position of the maximum-velocity radius in the annular channel with and without injection is in good agreement with the data of [3, 4].

The following coolant parameter values are taken in the calculations: $\nu^* = 0.173 \cdot 10^{-6}$; $\rho^* = 9.175$; $C_p{}^* = 5200$; $\lambda^* = 0.02$. The geometric dimensions corresponding to Figs. 1-5 are: $a^* = 5 \cdot 10^{-3}$ m, $b^* = 10 \cdot 10^{-3}$ m, $c^* = 12 \cdot 10^{-3}$ m, $x^*_L = 0.4$ m.

Flows with suction from the tube may occur with both reduction and increase in pressure (Fig. 2). With total suction from the channel, the dimensionless pressure difference is close to unity, which is in agreement with the experiments generalized in [5]. There is agreement between the theoretical pressure difference and the analytical dependence from [5] modified to take account of the possible variability of the suction rate over the length

$$\frac{2(P_T - P_{T_{in}})}{\bar{\rho}_T \bar{u}^2_{T_{in}}} = 1{,}3\left[1 - \left(\frac{\omega_T}{\omega_{T_{in}}}\right)^2\right] - \frac{\theta_{0T}}{3}\frac{x_L}{D_T}\frac{\omega_{T_{in}}}{\Delta\omega_T}\left[1 - \left(\frac{\omega_T}{\omega_{T_{in}}}\right)^3\right], \tag{19}$$

in which θ_{0T} is the hydraulic drag calculated according to the Blasius formula: $\theta_{0T} = 0.316\,\mathrm{Re}_T^{-0.25}$ and $\Delta\omega_T = \omega T_{in} - \omega T_L$.

The calculation of the pressure difference over the tube in injection is compared in Fig. 2 with the dependence [6]

$$\frac{2(P_T - P_C)}{\bar{\rho}_T \bar{u}^2_{T_{in}}} = 2{,}14\left(1 - \left(\frac{\omega_T}{\omega_{T_{in}}}\right)^2\right), \tag{20}$$

which is obtained on neglecting the viscous friction in the momentum-balance equation and is inaccurate for small injection rates; with increase in injection rate, the agreement between Eq. (20) and calculation improves. The calculation of the pressure difference over the length of the annular channel is compared with analytical dependences for the case of suction through the internal wall

$$\frac{2(P_C - P_{C_{in}})}{\bar{\rho}_C \bar{u}^2_{C_{in}}} = \left(1 - \left(\frac{\omega_C}{\omega_{C_{in}}}\right)^2\right) - \frac{x_L}{D_C}\frac{\omega_{C_{in}}}{\Delta\omega_C}\frac{\theta_{0C}}{3}\left(1 - \frac{\omega_C}{\omega_{C_{in}}}\right)^3\Bigg) \tag{21}$$

and for the case of injection

$$\frac{2(P_C - P_{C_{in}})}{\bar{\rho}_C \bar{u}^2_{C_{in}}} = 2{,}10\left(1 - \left(\frac{\omega_C}{\omega_{C_{in}}}\right)^2\right) - \frac{x_L}{D_C}\frac{\omega_{C_{in}}}{\Delta\omega_C}\frac{\theta_{0C}}{3}\frac{1}{(1 + b/c)} \times \left(1 - \left(\frac{\omega_C}{\omega_{C_{in}}}\right)^3\right) \tag{22}$$

in Fig. 3. Equation (21) is a modification of the formula used in [5] to approximate the experimental data on flow in a tube with unidirectional suction through a series of holes along its generatrix. The approximate Eq. (22) is obtained, like Eq. (20), by neglecting viscous friction at the permeable wall in the momentum-balance equation.

The dependences of the longitudinal pressure gradient on the intensity of the overflow in the circular and annular channels (Fig. 4) are similar if the measure of the overflow intensity adopted is $J_T = -v^a/u_T$, $J_C = bv^b/(c + b)u_C$. At small injection ($0 < J < 0.01$) linear relations give more accurate agreement with the calculation

$$\theta_T = 4C_{F_{T0}} + 13{,}3J_T,$$

$$\theta_C = 4C_{F_{C0}} + 12{,}4J_C.$$

Linear analysis of the dimensionless frictional factors in flow with injection through the permeable channel walls leads to the following laws

$$C_{F_T} = C_{F_{T0}} - 0{,}84J_T,$$

$$C_{F_C} = C_{F_{C0}} - 0{,}97J_C,$$

$$C_{F_b} = C_{F_{b0}} - 1{,}12\,\frac{v^b}{u_C}.$$

Linear approximation of the frictional factor with suction is less accurate than the quadratic approximation following from limiting theory [7]. Nevertheless, linear approximation may prove useful in view of its simplicity, for example, in solving so-called inverse collector problems: calculating the variation in channel cross section over the length necessary for the formation of the required suction-rate law. The aproximation of the frictional factor for the case of suction from the tube takes the form

$$C_{F_T} = C_{F_{T0}} - 1{,}55J_T.$$

The mean pressure over the volume flow rate

$$P_\Sigma = \frac{\omega_T}{\rho_T}\rho_\Sigma P_T + \frac{\omega_C}{\rho_C}\rho_\Sigma P_C \tag{23}$$

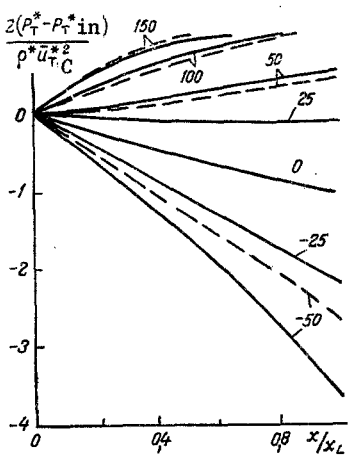

Fig. 2

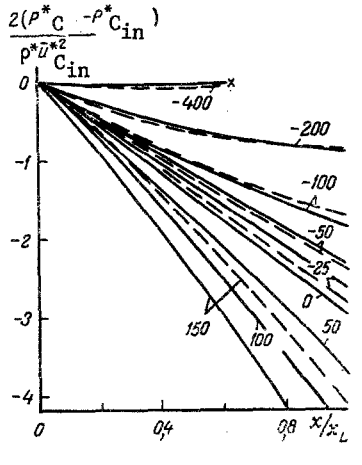

Fig. 3

Fig. 2. Pressure difference over the length of the permeable tube when $G^*_{Tin} = 0.2\cdot10^{-3}$ kg/sec, $K^* = 10^{-13}$ m^2. The continuous curves correspond to calculation and the dashed curves to Eqs. (19) and (20). The figures on the curves give values of Re_r.

Fig. 3. Pressure difference over the length of the annular channel with an internal permeable wall when $G^*_{Cin} = 0.8\cdot10^{-3}$ kg/sec, $K^* = 10^{-13}$ m^2. The continuous curves correspond to calculation and the dashed curves to Eqs. (21) and (22). The figures on the curve give values of Re_r; the cross corresponds to total suction from the channel.

is now introduced; the difference in this pressure characterizes the work done by the pressure forces per unit time in moving the coolant through the heat exchanger as a whole. The increment in this pressure consists of the increments required for injection along the channels and transverse to the permeable wall. Considering the isothermal case, and using the mass-balance Eqs. (4) and (5), the result obtained for the derivative $(P_\Sigma)_x'$ is

$$\frac{dP_\Sigma}{dx} = \omega_T \frac{dP_T}{dx} + \omega_C \frac{dP_C}{dx} - j(P_T - P_C). \tag{24}$$

The first two terms in Eq. (24) characterize the work for injection of the coolant along the channels and the third characterizes the work for injection through the porous wall. The expression for the derivative $(P_\Sigma)_x'$ may be written in a different form, using the total momentum-balance equation for both channels

$$\frac{d}{dx}\left(\frac{\beta_\Sigma}{\rho_\Sigma} + \overline{P}\right) = -\xi_\Sigma, \tag{25}$$

where β_Σ is the total momentum-flux coefficient over both channels

$$\beta_\Sigma = \frac{\omega_T^2 \rho_\Sigma}{S_T \overline{\rho_T}} \beta_T + \frac{\omega_C^2 \rho_\Sigma}{S_C \overline{\rho_C}} \beta_C,$$

and $\xi_\Sigma = \tau^a a + \tau^b b + \tau^c c$, $\overline{P} = S_T P_T + S_C P_C$.

Note that

$$P_\Sigma - \overline{P} = \left(\frac{\omega_T}{\overline{\rho_T}} \rho_\Sigma - S_T\right)(P_T - P_C) = \left(S_C - \frac{\omega_C}{\overline{\rho_k}} \rho_\Sigma\right)(P_T - P_C). \tag{26}$$

In the case of constant density ($\overline{\rho_T} = \overline{\rho_C} = \rho_\Sigma = 1$), using Eq. (26) and neglecting terms that contain derivatives of the momentum-flux coefficients β_T and β_C, it is found that

$$-\frac{dP_\Sigma}{dx} = \xi_\Sigma + \frac{d\beta_\Sigma}{dx} - \frac{d(P_\Sigma - \overline{P})}{dx} = \xi_\Sigma + j\left(\beta_C \frac{\omega_C}{S_C} - \beta_T \frac{\omega_T}{S_T}\right) + \frac{j^2}{KN_j} + \frac{(S_T - \omega_T)}{KN} \frac{dj}{dx}. \tag{27}$$

The difference in the mean pressure head $\overline{P}$ and the mean (over the volume flow rate) pressure P_Σ over the length of the porous section of cable is shown in Fig. 5. With increase in the overflow Reynolds number Re_r, the discrepancy between the differences $(\overline{P} - \overline{P}_{in})$ and $(P_\Sigma - P_{\Sigma in})$ increases; when $Re_r = 150$, the energy required for injection is approximately an order of magnitude greater than the analogous value for $Re_r = 0$. In the case where there is no

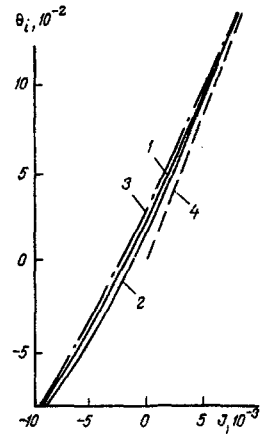

Fig. 4

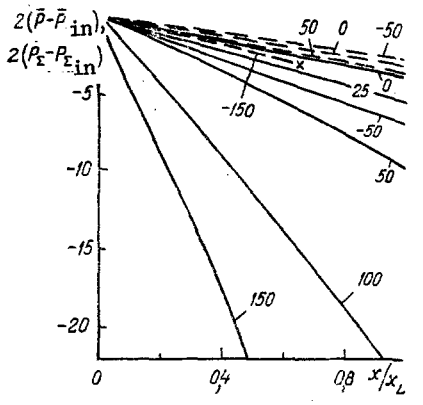

fig. 5

Fig. 4. Dependence of the hydraulic drag $\theta_{i,i=T,C}$ on the intensity of the overflow $J_{i,i=T,C}$: 1, 2) in the tube, $Re = 1.5\cdot10^4$ and $1.5\cdot10^5$, respectively; 3) in the annular channel, $Re = 1.5\cdot10^4$; 4) $\theta = 17.5$ J.

Fig. 5. Variation in mean pressure head $\bar{P}$ (dashed curves) and mean (over the flow rate) pressure P_Σ (continuous curves) over the length when $G^* = 0.1\cdot10^{-2}$ kg/sec; $K^* = 10^{-13}$ m^2; $\omega T_{in} = 0.2$; $\omega C_{in} = 0.8$. The figures on the curves are values of Re_r.

overflow, the differences in $\bar{P}$ and P_Σ are close, but not equal, in magnitude. The pressure $\bar{P}$ is introduced from the total momentum-balance equation for the two channels n and P_Σ from the kinetic-energy equation. These pressures are not identical even in the case of no overflow.

Analysis on the basis of the results obtained for individual terms in the total momentum-balance Eq. (25) shows that, in the given range of Re_r, the viscous and inertial terms in Eq. (25) are of the same order of magnitude; the variation in hydraulic drag is caused both by the change in viscous friction and by the change in the derivative of the momentum-flux coefficient.

NOTATION

x^*, longitudinal coordinate; r^*, radial coordinate; y^*, radial coordinate measured from the wall; u^*, v^*, longitudinal and radial components of the velocity vector; v_w^*, injection rate at the wall, positive in injection; P^*, pressure; ν^*, kinematic viscosity; ρ^*, density; $\rho^*_\Sigma = (\omega_T/\bar{\rho}^*_T + \omega_C/\bar{\rho}^*_C)^{-1}$, mean density over the flow rate; $\beta = \bar{u}^2/\bar{u}^2$, momentum-flux coefficient; $u_\tau^* = \sqrt{\tau^*/\rho^*}$, dynamic shear velocity; τ^*, tangential friction at the wall; D^*, channel diameter; K^*, permeability of wall, $\underline{K} = K^*/L^{*2}\ln(b/a)$; G^* total mass flow rate; $N = \underline{u}^*_\Delta L^*/\nu^*$, $R = \nu^{a*}a^*/\nu$, $Re_r = 2R$, $Re = u^*D^*/\nu^*$, Reynolds number; $C_{FT} = 2\tau^a/\rho_T u_T^2$, $C_F^b = 2\tau^b/\rho_C u_C^2$, $C_F^c = 2\tau^c/\rho_C u_C^2$, $C_{FC} = (bC_F^b + cC_F^c)/(b + c)$, friction numbers; $\theta = (2/\rho\bar{u}^2)(dP/d(x/D))$, local hydraulic drag; $(f_1, f_2, f_3)_{a,b,c}$ denotes f_1, f_2, f_3, respectively, in the regions a, b, c; $y^+ = y^*u_\tau^*/\nu^*$, $u^+ = u^*/u_\tau^*$, $v_w^+ = v_w^*/u_\tau^*$, hydrodynamic similarity variables. Indices: *, dimensional quantity; T, in tube; C, in annular channel; a, b, c, in the regions $0 \leq r^* \leq {}^a*$, $b^* \leq r^* \leq f^*$, and $f^* \leq r^* \leq c^*$, respectively; superscript a, b, c, at the walls $r^* = {}^a*$, $r^* = b^*$, and $r^* = c^*$, respectively; la, at the boundary of the laminar sublayer; E is the maximum-velocity pointl f, at $r^* = f^*$; in, in the initial cross section; L, at the end of the calculated section; 0, standard value; a bar above a quantity denotes averaging over the region.

LITERATURE CITED

1. N. M. Eroshenko and L. I. Zaichik, Hydrodynamics and Heat Transfer at Permeable Surfaces [in Russian], Moscow (1984).
2. G. K. Filonenko, Teploenergetika, No. 4, 40-44 (1954).
3. A. M. El-Nashar, Ind. Eng. Chem. Fund., 17, No. 3, 213-217 (1978).
4. N. M. Galin and V. M. Esin, Teplofiz. Vys. Temp., 14, No. 5, 991-997 (1976).
5. P. I. Bystrov and V. S. Mikhailov, Hydrodynamics of Collector Heat Exchangers [in Russian], Moscow (1982).

6. E. R. M. Olson and E. R. G. Ekkert, Prikl. Mekh., 33, No. 1, 7-20 (1966).
7. S. S. Kutateladze and A. I. Leont'ev, Heat and Mass Transfer and Friction in a Turbulent Boundary Layer [in Russian], Moscow (1972).

NONLINEAR MODEL OF THE INTERACTION OF CRYOAGENT FLOWS IN HEAT EXCHANGERS

I. K. Butkevich, M. A. Zuev, and V. F. Romanishin

UDC 621.594-71.045

A nonlinear analytical model of a two-flow heat exchanger is developed, ensuring high accuracy and speed, and universal indexing of the initial temperatures and eliminating degeneration of the heat transfer.

In investigating the cooling and heatingh of cryogenic systems, and in describing various transient conditions of quasistatic type, there arises the problem of correctly determining the functional relations between the limiting temperature of a two-flow heat exchanger.

Traditional methods of solving steady-heat-transfer problems reduce, as a rule, to two schemes. According to the first, the initial heat-transfer equations are integrated under the assumption of constant properties and parameters of the heat-carrier interaction. The limiting temperatures obtained here allow the mean values of the corresponding "constants" to be refined, after which the desired temperature values are redefined, and so on (linear-averaged model) [1, 2]. In practice, this scheme is a multistep iterative process.

The second calculation scheme reduces to direct integration of the heat-transfer equations on a computer, automatically taking account of the change in the coefficients at each step. The initial temperatures are specified here at one end of the heat exchanger.

Recently, combined calculation schemes have also appeared [3]; in these schemes, some of the deficiencies of linear models are eliminated in a narrow parameter range close to nominal conditions, as calculated by numerical integration.

Analysis of these methods leads to the conclusion that calculation by the first is faster than calculation by the second and is more flexible from the viewpoint of the possibility of determining an arbitrary pair of limiting temperatures. This is often decisive in the choice of an algorithm for investigating systems with parallel and series combinations of heat exchangers. However, the artificial linearization of the distributed parameters in the first method may lead to fundamentally incorrect solutions. This is associated with the possible disregard of those regions of the heat exchanger where nonlinearity of the thermophysical properties of the flows may lead to intersection of the temperature profiles, which would mean that the intermediate temperature differences vanish. In reality (if the influence of hydrayulic losses, external heat sources, and heat conduction is neglected), such degeneracy cannot occur. This physically impermissible phenomenon may be eliminated by developing a nonlinear model of heat transfer. In addition, it must be emphasized that the nonlinear terms of the equations describing processes in heat exchangers for the low-temperature region (T ~ 20-4.5 K) amount to tens of percent with respect to the linear terms, which also points to a need to develop a nonlinear theory of heat transfer.

Consider an initial system of steady equations of a two-flow heat exchanger, omitting the terms due to hydraulic losses, external heat sources, and heat conduction. The calculation of each of these factors falls outside the scope of the present work and may be accomplished by classical methods. The influence of these factors on the heat transfer is assumed to be small, and is easily taken into account by perturbation theory [1, 2] for the solution given below, which is expediently interpreted as the nonlinear zero approximation. Thus, fixing the flow rates and mean pressure in each flow for steady conditions, it is found that

Kriogenmash Scientific Design Department, Balashika. Translated from Inzhenerno-Fizicheskii Zhurnal, Vol. 51, No. 3, pp. 383-388, September, 1986. Original article submitted June 20, 1985.

0022-0841/86/5103-1023$12.50